Volumetric Medical Images Segmentation using Shape Constrained Deformable Models

Johan Montagnat, Hervé Delingette

Volumetric Medical Images Segmentation using Shape Constrained Deformable Models

J. Montagnat and H. Delingette

Projet Epidaure
I.N.R.I.A.
06902 Sophia-Antipolis Cedex, BP 93, France

Abstract

In this paper we address the problem of extracting geometric models from low contrast volumetric images, given a template or reference shape of that model. We proceed by deforming a reference model in a volumetric image. This reference deformable model is represented as a simplex mesh submitted to regularizing shape constraint. Furthermore, we introduce an original approach that combines the deformable model framework with the elastic registration (based on iterative closest point algorithm) method. This new method increases the robustness of segmentation while allowing very complex deformation of the original template. Examples of segmentation of the liver and brain ventricles are provided.

1 Introduction

We are interested in the extraction of geometric models of anatomical structures in medical images. Those models may be used for a surgery simulator with patient-specific data or the study of pathologies evolutions (deformations of ventricles in the brain...).

1.1 Related Work

Due to the low contrast of images we are considering, standard segmentation methods like thresholding or edge extraction perform poorly. Several optimized algorithms have been proposed:

- Segmentation can be achieved by *registration* of feature points [1], lines (such as crest lines [4]), surfaces or image volumes [10]. It may be difficult to extract feature points on complex shaped organs. We found that in the abdomen, the large variability in the relative location of the organs between patients made it difficult to perform a reliable registration.
- Some models built from *geometric primitives* have been proposed [11]. They tend to be very application specific and they apply only for simple shapes.
- The *active contour models* [6], known as *snakes*, have been widely used in 2D. Deformable surface models have been proposed [9] in 3D. In this paper we propose a similar approach with different constraints.

- *Parameterized models* [8] are very compact representations of the objects they represent. However, they are often limited in their shape description.
- *Statistical models* [2] use statistical information extracted from a training set to constrain the deformations of a model. The difficulty with this approach is the construction of a reliable training set, especially in 3D.

1.2 Contributions

In this paper, we are proposing an algorithm for extracting geometric models of anatomic structures from volumetric images. Our method combines the deformable model approach with the registration approach in order to improve the robustness of the segmentation.

Deformable models are well suited for the modeling of complex shapes because their shape description includes many degrees of freedom. However, if they are not submitted to global constraints, they can deform locally and they are not robust against noise, outliers or even natural shape variability.

On the other hand, the approach of registering a reference geometric model with a volumetric image tends to be more robust because it deforms the model on a global scale. However, the geometric transformation used for the registration is in general too restrictive to represent the inter-patient variation of anatomical structures. Furthermore, when the geometric transformation includes a large number of degrees of freedom, the numeric computation becomes unstable.

We propose a method that combines those two approaches. This hybrid mode of deformations consists in an additional external force acting on a deformable model. This force is derived from the best geometric transformation between the actual model shape and the closest data points. This scheme limits the degrees of freedom of the deformable model and improves the robustness of the segmentation.

2 Constrained Deformable Models

2.1 Deformable Models

We are using *2-simplex meshes* [5] to represent surfaces of $\mathbb{R}^3$. They are regular 3-connected meshes with interesting regularizing properties. Let $\mathcal{M}$ be a simplex mesh made of the vertices $\{P_i\}_i$ and $N_i, i \in [1;3]$ be three neighborhood functions. Each vertex P_i can be expressed as a function of its three neighbors, the three *metric parameters* ϵ_i^1, ϵ_i^2 and ϵ_i^3 and the *simplex angle* ϕ_i: $P_i = \epsilon_i^1 N_1(P_i) + \epsilon_i^2 N_2(P_i) + \epsilon_i^3 N_3(P_i) + L(N_1(P_i), N_2(P_i), N_3(P_i), \phi_i)$.

The metric parameters are barycentric coordinates locating the projection of P_i in the plane made by its three neighbors. The simplex angle describes the height of P_i above this plane. It is related to the notion of local discrete curvature of the surface. The metric parameters and the simplex angle describe the *shape* of a mesh with a given topology. This geometric description is up to a rigid or a scale transformation.

We can define the neighborhood of order s of a vertex P_i, $\mathcal{V}_s(P_i)$, as the set of points connected to P_i by a topological path of length lesser or equal to s.

We deform a mesh according to forces computed from the data. Thus, we need to extract some contour information to compute *external forces* applied to every vertices. We also need to apply regularizing or *internal forces* ensuring that deformations occur smoothly. Therefore we will express the total force applied on the vertex P_i by $f(P_i) = f_{int}(P_i) + \beta f_{ext}(P_i)$ where β is a weighting coefficient of external forces. The model iteratively deforms accordingly with Newtonian laws of motion: $P_i^{t+1} = P_i^t + \delta(P_i^t - P_i^{t-1}) + f(P_i)$ where δ is a damping factor between 0 and 1.

Contour Information Contours information is computed using the gradient as well as the grey level of voxels. The gradient of an image can be computed by applying Sobel masks or recursive filters. From the gradient we extract (i) a gradient map and (ii) an image of edges. The gradient map provides a local information indicating for each vertex the location G_i of the maximum gradient value in a restricted neighborhood of P_i. Edges are main contour points obtained by hysteresis thresholding of the gradient image. They are used to attract distant vertices toward boundary. For each vertex we are looking for the closest edge point E_i along the normal to the surface at this point.

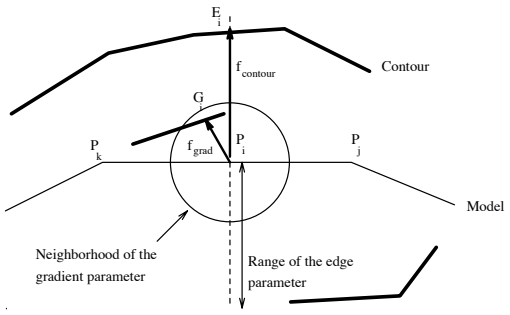

Fig. 1. Gradient and edges forces.

External Forces Computation We compute the external force applied on P_i as the weighted sum of the gradient force f_{grad} and the edges force f_{edge}. If we know the grey level range $[gmin; gmax]$ of the tissue to extract, we can use this information to exclude some outliers. $f_{ext}(Pi) = \rho_{grad}\tilde{f}_{grad}(P_i) + \rho_{edge}\tilde{f}_{edge}(p_i)$ with $\tilde{f}_{grad}(P_i) = f_{grad}(P_i)$ if $gmin \leq I(G_i) \leq gmax$ and is null otherwise; $\tilde{f}_{edge}(P_i) = f_{edge}(P_i)$ if $gmin \leq I(E_i) \leq gmax$ and is null otherwise. Since we are considering noisy data we may perform a smoothing of external forces over a neighborhood s. We then express the smoothed force applied on P_i by:

$$\bar{f}_{ext}^{s}(P_i) = \frac{1}{|\mathcal{V}_s(P_i)|} \sum_{P_j \in \mathcal{V}_s(P_i)} f_{ext}(P_j) \tag{1}$$

s acts as a *scale parameter* controlling the smoothing effect.

Regularizing Forces Computation Internal regularizing forces are related to the geometric properties of simplex meshes. They ensure smooth deformations of the surface. Using the scale parameter we want to control the extent of regularizing forces.

As shown before, the shape of a simplex mesh can be described by the metric parameters and the simplex angle at each vertex. Let us consider a mesh $\mathcal{M}$ with N vertices whose reference metric parameters are $\tilde{\epsilon}_i^1$, $\tilde{\epsilon}_i^2$, $\tilde{\epsilon}_i^3$ at the vertex P_i. We consider fixed the $\tilde{\epsilon}_i^j$ parameters so that only the simplex angle controls the regularity of the mesh at P_i. The regularizing forces then result in the minimization of the local energy $S_i = \frac{\alpha_i}{2}\|P_i\tilde{P}_i\|^2$ where α_i is a weight of the applied regularizing force and $\tilde{P}_i$ is the location of the point defined by the $\tilde{\epsilon}_i^j$ and $\tilde{\phi}_i$. Specifying the $\tilde{\phi}_i$ value set the $\tilde{P}_i$ location and therefore the resulting internal force $f_{int}(P_i) = \frac{\partial S_i}{\partial P_i} = \alpha_i P_i\tilde{P}_i$.

2.2 Shape constraint

Let us consider a *reference shape* for a given mesh $\mathcal{M}$ described by the simplex angles $\{\phi_i^0\}_i$. Setting $\tilde{\phi}_i = \phi_i^0$ for each i, we force the vertices to evolve toward their reference shape. Thus, a mesh evolving under the only regularizing forces will eventually come back to its reference shape. Figure 2 illustrates a deformed model of a face retrieving its reference shape under shape constraints.

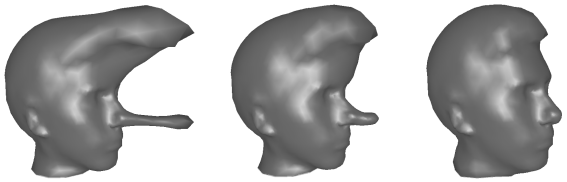

Fig. 2. Model of a face evolving under a shape constraint

We added a scale parameter so that all neighbors in an order s neighborhood are implied in the computation of shape constraint regularizing forces. Given a reference shape defined by $\{\phi_i^0\}_i$ we express $\tilde{\phi}_i$ as an offset from its reference value:

$$\tilde{\phi}_i = \phi_i^0 + \sum_{P_j \in \mathcal{V}_s(P_i)} \lambda_{ij}(\tilde{\phi}_j - \phi_j^0) \tag{2}$$

We proved that $\tilde{\phi}_i$ iteratively converges toward ϕ_i^0 as soon as $\sum_j \lambda_{ij} = r < 1$. We shall therefore consider $\forall i \forall j, \lambda_{ij} = \frac{r}{|\mathcal{V}_s(P_i)|}$ with r constant.

A simple test shows that the scale parameter leads to a more global behavior of the surface while deforming. Figure 3 (left) represents a synthetic cross model which has been rotated and translated away from its reference location. The model is then attracted toward its reference position by the wireframed cross.

Under the external forces, the surface locally deforms. After a given number of iterations, we can evaluate the distance between the model $\{P_i\}_i$ and its reference position $\{P_i^0\}_i$: $d\left(\{P_i\}_i, \{P_i^0\}\right) = \sum_i \|P_i - P_i^0\|^2$.

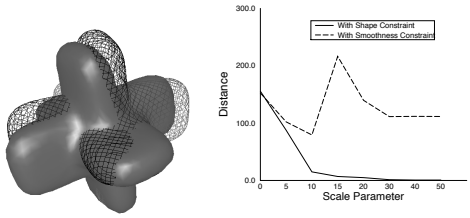

Fig. 3. Displaced cross model and distance after deformation

Figure 3 (right) shows the distance between the deformed model and the reference position as a function of the scale parameter. It can be seen that the distance consistently decreases when the scale parameter increases. It means that with a higher scale parameter (a wider smoothing over the surface), the shape is better preserved during the deformation. The graph also shows that the deformation is far better with the shape constraint (the solid line) than the simplex angle continuity constraint (the dashed line).

The shape constraint scheme provides a very interesting behavior: when data is missing, the model tends to deform toward a given shape corresponding to an a priori knowledge of the organ shape.

2.3 Global Transformation

Another way of deforming the model is to use only global transformations to drastically reduce the space of allowable deformations. Thus the model can be registered as closely as possible to some data points by a global transformation f.

Consider the pair of points $\{(P_i, D_i)\}_i$ where $D_i = P_i + \bar{f}_{ext}^s(P_i)$ (see eq. 1). We are looking for a global transformation f that minimizes the squared distance between P_i and the corresponding D_i:

$$f = \arg\min_{g \in F} \left\{ \sum_{i=1}^{N} \|g(P_i) - D_i\|^2 \right\} \tag{3}$$

where F is a functional space limiting the kind of deformation allowed. We have been investigating the function spaces: F_{rig} (rigid transformations), F_{sim} (similarities i.e. rigid transformations with a scale factor), F_{aff} (affine transformations) or F_{spl} (cubic B-spline transformations). They are ranked into increasing number of degrees of freedom since $F_{rig} \subset F_{sim} \subset F_{aff} \subset F_{spl}$. Details on resolving equation 3 can be found in [7] for g in F_{rig}, F_{sim} or F_{aff} and in [3] for g in F_{spl}.

More complex, transformations could have been introduced. However, the evaluation of the best cubic B-spline transformation is already much more costly than the other transformations. It would be even more time consuming to evaluate transformations with more freedom degrees (such as higher order B-splines), not to mention numerical instabilities of the resolution method. In practice, we are limited in the set of usable global transformations.

2.4 Hybrid Models

We now have a locally regularized deformable model scheme and a set of global transformations varying from completely rigid to cubic B-spline transformations. Local deformations are often under-constrained: the model bends too freely and is too sensitive to outliers. Global transformations do not allow the model to fit the set of morphological variations of some human organs and it cannot be extended due to computation time and numerical stability problems.

We propose an hybrid model combining the advantages of both approaches. Given a deformation field of external forces $\{\bar{f}^s_{ext}(P_i)\}_i$, we can compute a global transformation f. This global transformation results in the application of a force $f^s_{global}(P_i)$ to each vertex of the mesh. $f^s_{global}(P_i)$ equals to the displacement of P_i under the global transformation f. As shown in figure 4, we apply on P_i a weighted average of the local and the global force.

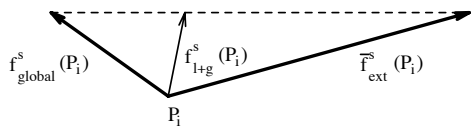

Fig. 4. Hybrid force computed from local and global deformations

The hybrid force applied on P_i is written $f^s_{l+g}(P_i) = \gamma \bar{f}^s_{ext}(P_i) + (1-\gamma) f^s_{global}(P_i)$ where γ is a *locality parameter*. The figure 5 shows a part of a synthetic cross model deforming under the local, hybrid and global schemes. The cross model has been rigidly moved away from its reference location. A wireframe cross at the reference position attracts the model back to its original position using completely local deformations (left), hybrid deformations based on a rigid global transformation (center) and rigid transformations (right).

We obtain a trade off between local deformation and global transformation using the hybrid scheme. In the local case, the vertices locally deform and the shape is strongly disturbed. In the global case, the shape remain untouched. In the hybrid approach (here using $\gamma = 20\%$) we have an intermediate behavior.

Since the locality factor plays a role similar to the scale parameter (a larger scale implies a more global behavior), we can bind γ and s: $\gamma = (1 - s/Nmax)^3$ where $Nmax$ is the maximal neighborhood size.

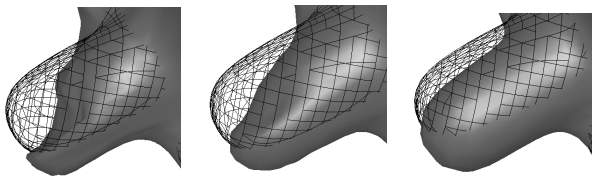

Fig. 5. Effect of local, hybrid and global deformations after a few iterations

3 Segmentation using Deformable Models

Organs segmentation from volumetric medical images if often a required stage for further analysis. Segmentation of the liver and vascular trees from abdominal CT-scan images is needed for laparoscopic surgery simulation. Study of brain ventricles deformations is also relevant for diagnosis of brain pathologies. For the liver, we use a template semi-automatically extracted from the NLM (*National Library of Medicine* data. For the ventricles we built a template from a brain segmented by hand.

The segmentation process requires two stages. The Initialization locates and scales the template of the organ we are considering inside the volumetric image. From this rough initial position, the model locally deforms using the hybrid constraints described above. The segmentation is achieved when the model stops deforming.

3.1 Initialization

We need a first segmentation to initialize the mesh location. It can be obtained by a first very rough segmentation of the organ, using standard segmentation methods such as thresholding or isosurface extraction. Once we have an approximative contour, we deform our model to fit it. Since we are relying on a shape constraint in the following stage, we must strongly constrain deformations so that we keep an overall consistent shape.

We use the global deformation scheme described above to initialize the model. Thus we constrain allowable deformations in functions classes we have been investigating. We just need to match each vertex of the model P_i with a point of the rough contour extracted. We use the Iterative Closest Point algorithm (ICP) [12] to do so. Figure 6 illustrates the slice of a liver model before and after ICP using an affine transformation constraint.

The rough contour has been obtained by thresholding the data. The regular contour is the 2D trace of the model in the given slice. To obtain better matches in the ICP algorithm (and therefore better global transformation evaluation) we first evaluate the best rigid transformation, then we add degrees of freedom by using the best similarity and finally the best affine transformation.

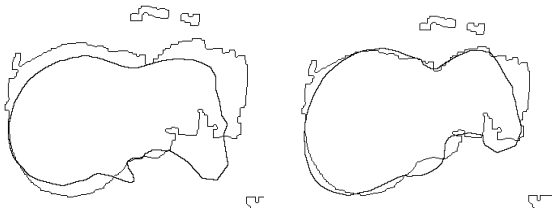

Fig. 6. A slice of the liver before (left) and after (right) affine registration

3.2 Deformation

Once the model has been initialized, we compute the deformation field from the image and we deform the model using the hybrid formulation using B-spline global transformations and regularizing shape constraints. The local force applied on each points is $f^s(P_i) = \bar{f}^s_{int}(P_i) + \beta\left(\gamma \bar{f}^s_{ext}(P_i) + (1-\gamma) f^s_{spline}(P_i)\right)$. The use of the hybrid model is required to control deformations since the initialization stage provide such a rough starting point. Applying only local deformations would lead the model to deform toward outliers.

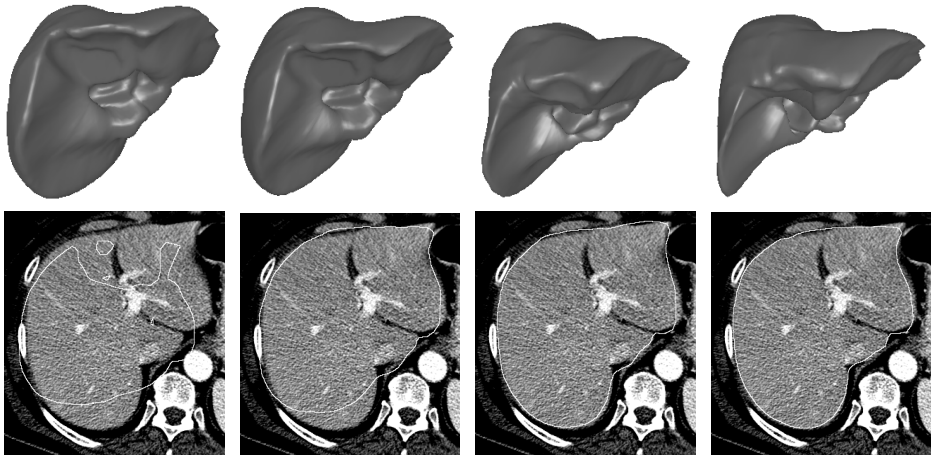

Fig. 7. Deformation of a liver model

3.3 Results

We applied our deformation scheme on abdominal CT-scans (to extract the liver) and MRI brain image (to extract ventricles). Figure 7 shows each step of the segmentation process on a liver model. Up row is the initial model (left) and

the model after the initialization stage (center-left). Only affine transformations were allowed so the overall shape is almost identical. A slight variation of the orientation can be seen though. The model is then strongly constrained (center-right) with a low locality factor so that it deforms toward edges without being sensible to outliers. As the registration of the model with the image gets better, constraints are released (right) by increasing locality to let the model deform more locally. Bottom row of figure 7 shows the evolution of the intersection of the model with one slice of the data.

Figure 8 shows the template of ventricles before (left) and after (right) the segmentation process. As expected, the overall shape of the organs has been

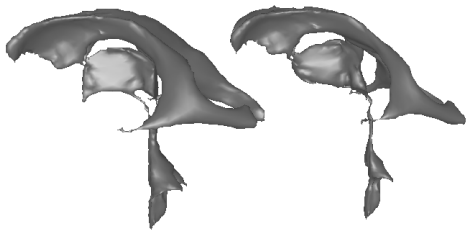

Fig. 8. Model of the ventricles before (left) and after (right) deformation

preserved. The figure 9 shows the intersection of the liver and ventricles models on different slices of the original data.

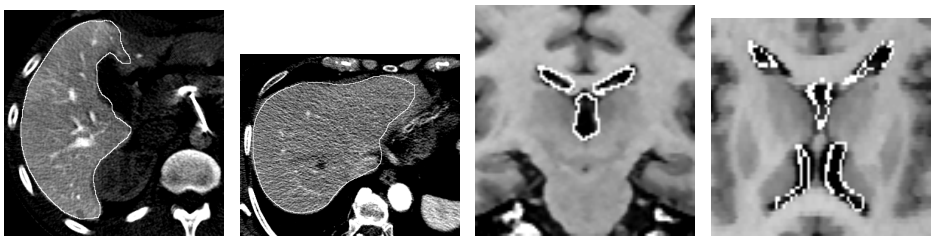

Fig. 9. Slice of recovered liver (left) and ventricles (right) models

4 Conclusion and Future Work

We have explained how to build deformable models and how to compute a set of deformations varying from rigid to completely local transformations. Using the hybrid deformation approach the model takes advantage of both global and local deformation schemes. Such constrained model provides an accurate mechanism to perform segmentation in low contrasted medical images.

In the future we plan to improve segmentation accuracy by using statistical information for locally controlling the deformation parameters. Our segmentation tool allows the construction of anatomical databases. From those databases

we can study morphological variations of organs. Another possible use of databases is the study of pathologies evolution or organs growth.

Acknowledgment

The authors are grateful to J. Marescaux, J.M. Clément and V. Tassetti from the *IRCAD* (Institut de Recherche sur les Cancers de l'Appareil Digestif, Strasbourg, France) for their collaboration in building the liver model and providing the abdomen CT-Scans. We thank Ron Kikinis from the Brigham and Women's Hospital, (Boston, USA), for providing the MRI images of the head. We also thank the members of the Epidaure project for their previous work, criticism and proof reading.

References

1. J. Boes, C. Meyer, and T. Weymouth. Liver definition in CT-using a population based shape model. In *Computer Vision, Virtual Reality and Robotics in Medicine*, volume 905 of *Lectures Notes in Computer Science*, pages 281–286. Springer-Verlag, Apr. 1995.
2. T. Cootes, C. Taylor, D. Cooper, and J. Graham. Active shape models, their training and application. In *Computer Vision and Image Understanding*, volume 61, pages 38–59, Jan. 1995.
3. J. Declerck, J. Feldmar, M. Goris, and F. Betting. Automatic registration and alignement on a template of cardiac stress and rest SPECT images. Technical Report 2770, INRIA, Jan. 1996.
4. J. Declerck, G. Subsol, J. Thirion, and N. Ayache. Automatic retrieval of anatomical structures in 3D medical images. In N. Ayache, editor, *Computer Vision, Virtual Reality and Robotics in Medicine*, volume 905 of *Lecture Notes in Computer Science*, pages 153–162, Nice (France), Apr. 1995. Springer Verlag.
5. H. Delingette. Simplex Meshes: a General Representation for 3D Shape Reconstruction. Technical Report 2214, INRIA, Mar. 1994.
6. M. Kass, A. Witkin, and D. Terzopoulos. Snakes: Active Shape Models. *Intertnational Journal of Computer Vision*, 1:321–331, 1987.
7. X. Pennec. *L'incertitude dans les Problèmes de Reconnaissance et de Recalage. Application en Imagerie Médicale et Biologie Moléculaire*. PhD thesis, Ecole Polytechnique, France, 1996.
8. G. Székely, A. Kelemen, C. Brechbüler, and G. Gerig. Segmentation of 2D and 3D objects from MRI volume data using constrained elastic deformations of flexible Fourier surface models. *Medical Image Analysis*, 1(1):19–34, July 1996.
9. D. Terzopoulos, A. Witkin, and M. Kass. Constraints on Deformable Models: Recovering 3D Shape and Nonrigid Motion. *Artificial Intelligence*, 36(1):91–123, 1988.
10. J.-P. Thirion. Non-Rigid Matching using Demons. In *Computer Vision and Pattern Recognition, CVPR'96*, San Francisco, California USA, June 1996.
11. A. Yuille and P. Hallinan. Deformable templates. In M. Press, editor, *Workshop on Active Vision*, 1991.
12. Z. Zhang. Iterative point matching for registration of free -form curves and surfaces. *International Journal of Computer Vision*, 13(2):119–152, Dec. 1994.